GEOPHYSICS, VOL. 79, NO. 4 (JULY-AUGUST 2014); P. B187–B199, 8 FIGS., 2 TABLES.
10.1190/GEO2013-0256.1

Case History

Assessment of near-surface mapping capabilities by airborne transient electromagnetic data — An extensive comparison to conventional borehole data

Cyril Schamper[1], Flemming Jørgensen[2], Esben Auken[3], and Flemming Effersø[4]

ABSTRACT

A newly developed helicopter transient electromagnetic (TEM) system has the ability to measure very early times within just a few μs after the turn off of the primary current. For such a system, careful calibration and accurate modeling of the electromagnetic (EM) response is critical to get true resistivities of the very shallow geologic layers. We discovered that this leads to resolution of the same level or in some cases even better than what can be obtained from airborne frequency EM systems. This allowed a range of important applications where high and accurate resolution is mandatory, e.g., geotechnical applications such as urban planning, railroad and road investigations, landslides or distribution of raw materials, and assessing aquifer vulnerability. We evaluated the results of a pilot survey covering the Norsminde catchment south of Aarhus, Denmark, where we found that near-surface layers (top 30 m) can be mapped with an accuracy of a few meters in a complicated glacial sedimentary environment. The mapping of the geologic layers was assessed by a detailed analysis in which we developed a general methodology for crosschecking the EM and borehole data. This methodology is general and can easily be adapted to other data types and surveys. After rating the quality of the boreholes based on a list of predefined criteria, we concluded that the EM data matched with about three-quarters of the boreholes located within less than 15 m from the closest EM soundings. The remaining quarter of the boreholes fell into two groups in which half of the boreholes were of very poor quality or had inaccurate coordinates. Only eight of all the boreholes could not be reproduced by the data, and we attributed this to be caused by very strong lateral or vertical geologic variations not resolvable by the TEM technique.

INTRODUCTION

Through the last few decades, electrical and electromagnetic (EM) methods have been constantly improved with the purpose of delivering detailed and reliable information about near-surface geology. Review papers by Dahlin (2001) for direct current (DC) methods and Tekzan (1999) and Everett (2012) for induction EM methods provide overviews of the large range of applications in which near-surface geologic information is useful. Among the most recent studies, one can find various applications such as aquifer vulnerability mapping (Röttger et al., 2005), landslide hazards (Pfaffhuber et al., 2010; Supper et al., 2013), clay mapping (Donohue et al., 2012), agriculture regulation (Refsgaard et al., 2014), and overburden mapping (Schamper et al., 2012; Oluwafemi and Oladunjoye, 2013). Most of those studies rely on the mapping of clay geologic units because of their particular mechanical and hydraulic properties, which play key roles in geotechnical (e.g., landslides, construction) and hydrogeological (e.g., groundwater flow modeling, pollution plumes) problems. These clay units generally have high electrical conductivity values, which make them excellent

Manuscript received by the Editor 9 July 2013; revised manuscript received 22 January 2014; published online 4 June 2014.
[1]Formerly Aarhus University, Department of Geoscience, Aarhus, Denmark; presently Sorbonne Universités, UPMC Univ Paris 06, Paris, France. E-mail: cyril.schamper@upmc.fr.
[2]Geological Survey of Denmark and Greenland, Højbjerg, Denmark. E-mail: flj@geus.dk.
[3]Aarhus University, Department of Geoscience, Aarhus, Denmark. E-mail: esben.auken@geo.au.dk.
[4]SkyTEM Surveys ApS, Aarhus N, Denmark. E-mail: fe@skytem.com.

targets for mapping with EM methods. When ground-based EM methods are inexpensive compared to operating a helicopter or an airplane and allow accurate and advanced studies of specific sites, they do not scale well when the surface to be covered is large, i.e., above hundreds of square kilometers or along transects several kilometers long. In these cases, airborne methods constitute a cost-efficient alternative estimated to be a factor 7–8 times less expensive where the line distances are the same, but the airborne EM (AEM) method has a factor of 7 more soundings along the flight lines.

Helicopter frequency EM (HFEM) systems have been used more for near-surface mapping than helicopter transient EM (HTEM) systems because they traditionally have a higher frequency content and a more compact geometry, which plays a role in the lateral and vertical near-surface resolution of the geologic layers. For deeper targets, HTEM systems have been preferred to HFEM systems as most HFEM systems cannot reach depths much below 100 m. Thorough discussions of HFEM systems for near-surface mapping, e.g., groundwater exploration, can be found in Steuer et al. (2009). To get an equivalent high-frequency content, HTEM systems must be able to measure very early off-time gates right after a short turn-off of the current in the transmitter loop and this has hitherto been a difficult technological challenge.

The SkyTEM system (Sørensen and Auken, 2004), initially designed for groundwater mapping, has been constantly improved during the last decade, one of the most important ameliorations being the measuring of earlier and earlier gates (Auken et al., 2010). These developments led to the construction of a new version of the system SkyTEM101, which has been used for mapping an entire catchment with focus on aquifer delineation and geologic mapping in the top 30 m (Schamper and Auken, 2012). The aim of this paper is to assess the near-surface resolution capabilities of this system by comparing to borehole data.

Most papers discussing AEM and borehole data consider a relatively limited number of boreholes (Baldridge et al., 2007; Dickinson et al., 2010). Extensive and detailed comparison can be found in Lane et al. (2001) and Mullen et al. (2007). In these studies, they compared results from TEMPEST surveys applied to salt mapping with conductivity logs. They showed good resemblances especially for layers with low resistivities in the range of 1–10 Ωm. In the present study, there is no salt water intrusion and resistivities are more often in the range of tens of Ωm, making the resolution of layers more challenging for the system. Also, conductivity logs, despite their own uncertainty coming from local geologic heterogeneity, disturbances due to the drilling technique and problematic calibration, provide more quantitative information compared to geologic logs, but they are not always available. In the present comparison, the survey area contains more than 500 boreholes, but only a few usable conductivity logs are present and only three are close to the flight lines. In contrast to the study by Lane et al. (2001) where line spacing was 200 m, the spacing reached with the new HTEM system is down to 50 m in the most geologically complex area. Moreover, the HTEM system is more compact compared to a fixed-wing system such as TEMPEST where the receiver loop is towed about 100 m behind the transmitter frame. Our comparison is therefore focused only on boreholes very close to flight lines (<15 m), and we illustrate the difficulties in comparing site-specific detailed geologic information with geophysical models, which often integrate larger volumes of the subsurface. To take benefit from a conventional borehole database, we propose a methodology where we consider all boreholes with a lithological and/or a geologic description. Our methodology consists of two main steps: (1) assessment of borehole quality and (2) crosschecking the match between boreholes and AEM data based on quantitative parameters.

In the following, we will present the HTEM system and focus on the most important features for the interpretation of early time data. A preliminary sensitivity analysis is carried out to assess the performance of the HTEM system compared to a HFEM system (like RESOLVE) for resolving thin near-surface layers. Subsequently, the pilot survey area and the geophysical results of the campaign are introduced. Finally, a comparison between the AEM resistivities and borehole data is made to test and validate the efficiency of the system for mapping and resolving the top 30 m of near-surface geology.

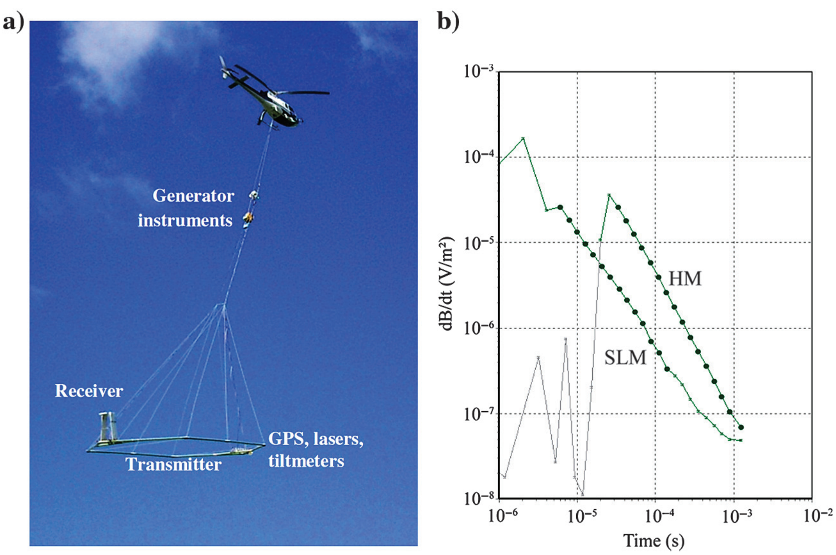

Figure 1. (a) The SkyTEM101 system in operation and (b) a classical dual-moment dB/dt sounding curve with SLM and HM curves; the circles indicate the times (from the beginning of the turn-off ramp) that are actually used for the interpretation of the data.

A TRANSIENT AEM SYSTEM FOR NEAR-SURFACE MAPPING

Technical specifications

The new SkyTEM101 is shown in Figure 1a. The main new feature of this system is the capability to measure very early times at only a few µs from the end of the turn off (Schamper and Auken, 2012; Schamper et al., 2014), which to our knowledge has not been measured by any other transient AEM system before. The system has a small transmitter loop area of only 130 m^2 and uses two transmitter moments (Figure 1b); the superlow moment (SLM) with an injected current of 7 A and the high moment (HM) with a larger current of 55 A. The SLM is meant for very short turn offs of the current in the order of ~3 µs and makes it possible to measure very early times a few µs after the end of the ramp. Low-pass filters of 300 and 450 kHz are introduced by the receiver coil and the transmitter, respectively. In contrast, the HM with a turn off time of ~12 μs allows later times measurements, resulting in a deeper depth of investigation (DOI). The recorded times span from 2 to 3 μs to slightly more than 1 ms after the end of the turn off ramp, giving a DOI slightly more than 100 m for an average ground resistivity of 50 Ωm.

The small size and weight of the system allows the use of a smaller and more cost-effective helicopter. The frame is made from a new composite material, and the aerodynamics profile allows the system to be flown at a speed of 100–140 km/h. In our case, it took one week to fly the pilot survey of ~2000 line km over an area of 120 km^2 with a line spacing of 50–100 m. This time includes refueling of helicopter, check and small repairs of the system, delays due to weather conditions etc.

In the acquisition settings of the present survey, each moment, SLM and HM, had a stack size of 80 transients with a repetition frequency of 400 Hz resulting in a full sounding for each 0.6 s. With an average flight speed of 30 m/s, this gives a full SLM + HM sounding for each 15 m. An additional stacking window is applied to the data during processing to improve the signal-to-noise ratio at late times. The width of the stacking filter varies and increases with gate times to obtain the best lateral resolution possible; it is shorter at earlier gate times, starting with 1 s for gates until 20 μs. The final best lateral resolution of the top 30 m is estimated at ~20–40 m, considering the diffusivity of the method, the frame altitude close to 30 m and a conductive ground. For a more resistive ground, the footprint of the system becomes larger (Reid and Vrbancich, 2004), and a larger volume of the ground is averaged.

System calibration and coil response

The improvement of the electronics to get the very short turn off (which is equivalent to getting high-frequency content in the frequency domain) is not sufficient by itself, and careful processing procedures have to be applied to interpret those early times correctly.

During the last decade, extensive efforts have been made to calibrate the various AEM systems on the market to deliver a quantitative estimation of the ground resistivity for low to moderate resistivities, i.e., between 1 and 200 Ωm (Vrbancich and Fullagar, 2004, 2007; Lavoué et al., 2010; Podgorski et al., 2013). For the SkyTEM101 system, we have applied the calibration procedure detailed in Foged et al. (2013). In short, this consists in measuring the ground response at a reference site where the resistivity model is well documented, e.g., by boreholes (drill description and electrical log [Ellog] if available), electrical resistivity tomography, and/or ground-based geophysical methods. The measured sounding curve is shifted in amplitude and time to match the forward EM response of the reference model. The calibration usually results in an amplitude correction factor close to 1.0 (generally in the range 0.95–1.05), and in a time shift correction close to 0 μs (generally within ± 2 μs). For the resolution level targeted for this study, timing is crucial to a level less than a microsecond as even a shift in the order of ±1–2 μs has shown to change the interpretation of the top 5–10 m significantly. Linking this to geology, a sandy layer would be replaced by a clayey layer for a positive time shift and inversely for a negative shift (Schamper et al., 2011).

Off-time gates measured at few μs after the turn-off of the current are disturbed by what is denoted as the *coil response* (CR). The CR is generated by residual currents circulating in the transmitter loop after the current turn off. To minimize the CR amplitude compared to the ground response, the receiver loop of the system is placed slightly outside the transmitter wire (Figure 1a). However, the CR still needs to be modeled to be able to use the very early times of the system. The procedure detailed in Schamper et al. (2014) is applied, allowing the usage of gates 2–3 μs from end of ramp, i.e., 5–6 μs from the beginning of ramp with a ramp time of ~3 μs.

Sensitivity and performance analysis based on synthetic cases

To demonstrate the resolution capabilities from a pure theoretical point of view, we have carried out a sensitivity analysis on the estimation of the thickness or depth of a near-surface layer. To put the resolution capabilities in perspective, the transient EM data are compared to the well-known frequency EM system RESOLVE (CGG). The RESOLVE system has a total of six frequencies: 0.395, 1.8, 3.2, 8.2, 38.8, and 129 kHz. A nominal flight altitude of 30 m is considered. Because the focus is on very near surface information and to keep the analysis simple, a constant relative data error of 2% is assigned to all times and frequencies.

Similarly to the work of Tarantola and Valette (1982) and Auken and Christiansen (2004), a standard deviation factor (STDf) is estimated from the linearized approximation of the covariance matrix of the estimation error. Under lognormal approximation and for a parameter whose estimation equals q, it is 68% likely that the parameter lies in the interval $q/\mathrm{STDf} < q < q.\mathrm{STDf}$. The results of this analysis are displayed in Figure 2. For the present study, the embedding media has a fixed medium resistivity of 100 Ωm. In Figure 2a, a two-layer model is considered with varying parameters: the resistivity of the first layer (ρ_1) from 1 to 1000 Ωm and the thickness of the same layer (h_1) from 1 to 20 m. STDf values close to 1 (dark blue) mean that the thickness of the top layer is very well resolved. For instance, a STDf of 1.5 indicates an error of about ±50%. When ρ_1 is close to the surrounding resistivity of 100 Ωm, a clear axis of nondetermination is visible, as the first layer is confounded with the second layer in terms of resistivity. Figure 2a shows that the area of low determination (dark red) is larger for RESOLVE compared to SkyTEM101 for resistivities below the background resistivity. For a top layer more resistive than the background, the HFEM system is performing slightly better than the HTEM system. The plot for the HTEM system indicates that the thickness of layers at least 3 m thick is well determined ($\mathrm{STDf} < 1.5$) for resistivities below 20 Ωm (background of 100 Ωm). The more ρ_1 is lowered, the thinner the top layer can be resolved, with 1-m-thick layer being well determined for ρ_1 of few Ωm. As expected, above 100 Ωm, the resolution of a more resistive layer is more difficult, whatever the value of ρ_1. In this case, the top layer needs to be at least 4 m thick to be well resolved.

Figure 2b–2e deals with the cases of a dipping near-surface layer of a thickness of 1, 2, 5, and 10 m, respectively. As with Figure 2a, the plot for the RESOLVE configuration shows an area of low determination (dark red) slightly larger compared to the SkyTEM101 configuration for 1 and 2 m cases (Figure 2b and 2c). For the 5 and 10 m cases (Figure 2d and 2e), the overall performances of both systems are similar. Analysis of the SkyTEM101 plot concludes that the location of layers less than 2-m deep is approximate. Contrary to the two-layer model, the three-layer, or sandwich, model clearly shows that thin layers have to be more conductive than the surrounding layer to be well resolved. The enlarging area of accurate determination (dark blue) from 1- to 2-, 5-, or 10-m-thick

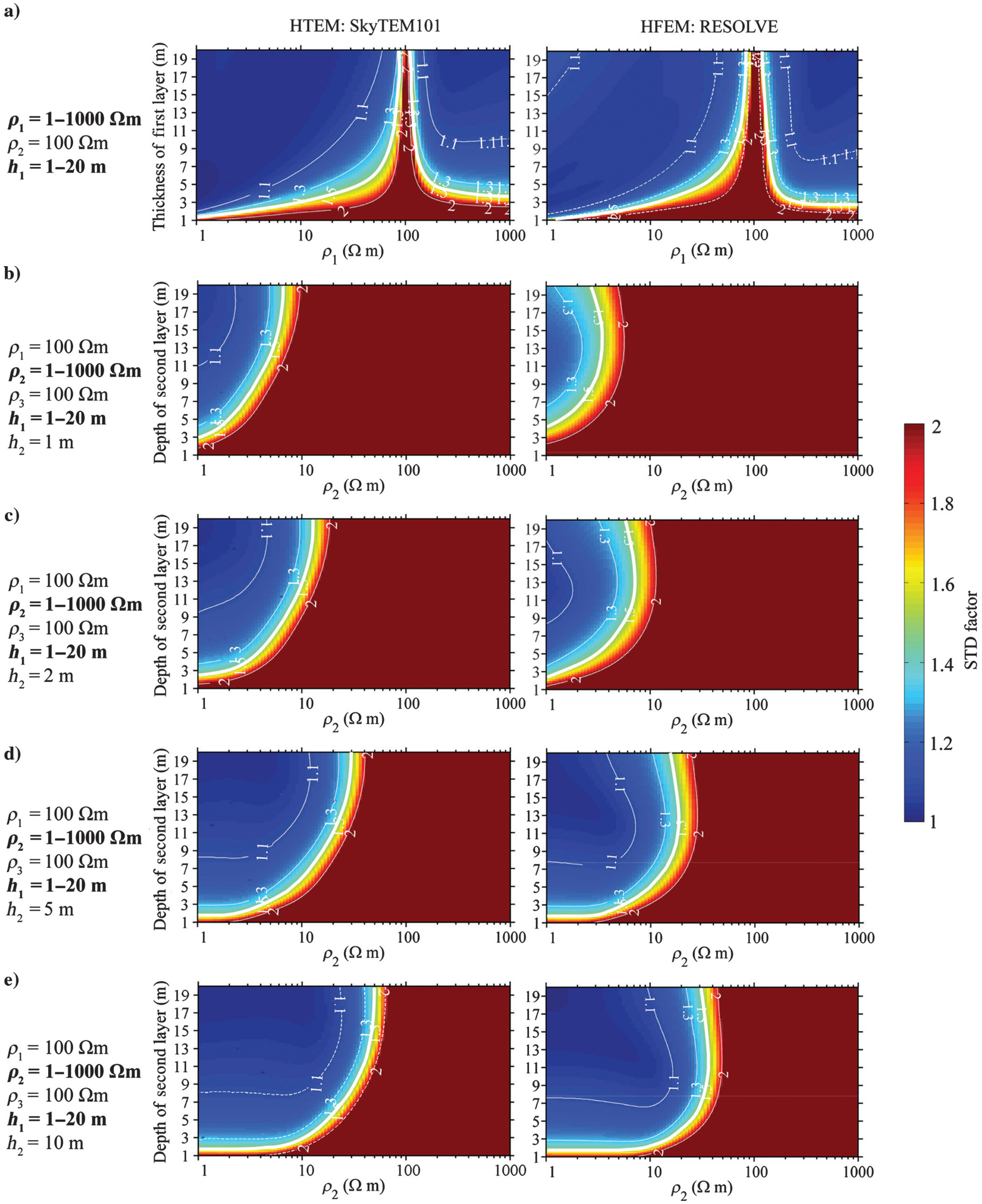

Figure 2. Comparison of SkyTEM101 and RESOLVE sensitivities to the near surface regarding the estimation of (a) the thickness of a first thin layer, (b) the depth of a 1-m-thick layer, (c) the depth of a 2-m-thick layer, (d) the depth of a 5-m-thick layer, and (e) the depth of a 10-m-thick layer. Plotted values correspond to the estimation of the error in terms of STDf. Well-resolved thicknesses or depths correspond to STDf close to 1. The thick white line corresponds to the isoline with a STDf value of 1.5.

layer (Figure 2b–2e) illustrates the importance of the conductance, i.e., the product of conductivity and thickness, for the visibility of the layer. For a 2-m-thick layer at a depth of 20 m, ρ_2 has to be $< \sim 15\ \Omega$m for thin layer to be well resolved. For the 5- and 10-m-thick layers (Figure 2d and 2e), the thresholds are 30 and 50 Ωm, respectively.

The analysis presented in Figure 2 shows the competitive performance of the HTEM system compared to a HFEM system for the resolution of the near surface. We are aware that the analysis does not consider all field parameters such as systematic errors at early times or high frequencies, altimeter errors etc. (Christiansen et al., 2011). However, it increases the interest of continuing the study of the HTEM system and investigating what can be achieved from field data.

THE AEM SURVEY: SURVEY DESIGN AND INVERSION RESULTS

The development of the SkyTEM101 system is part of the NiCA project (Nitrate Reduction in a Geologically Heterogeneous Catchment, Danish Council for Strategic Research) whose main objective is to model and estimate the nitrate reduction in shallow aquifers (top 30 m) at the scale of an entire catchment and at the resolution of each farm field (Refsgaard et al., 2014).

The survey area is located 20 km south of Aarhus, Denmark and covers the Norsminde catchment area of about 120 km^2. Figure 3a shows the different phases of the survey with flight lines totaling approximately 2000 line km. A first phase of lines was flown with a line spacing of 100 m (black lines in Figure 3a), then a second set was added in the western part of the area (orange lines in Figure 3a) also with a line spacing of 100 m, but between phase 1 lines, and finally, a last small group of crosslines (green lines in Figure 3a) was produced with a 50-m line spacing. As a result, the western area common to phases 1 and 2 has a line spacing of 50 m.

As mentioned earlier, the sounding spacing of individual AEM soundings along the lines is about 15 m with a cruise speed of 100 km/h. The lateral resolution is finest in the near surface (top 30 m) and becomes gradually coarser with depth. With a nominal flight height of 30 m for the frame, the best expected lateral resolution for the system is 20–40 m. Another characteristic of AEM data, which impacts the resolution, is the EM coupling due to the presence of man-made installations such as buried cables along roads or power lines. Coupled data cannot be compensated and must be culled (Viezzoli et al., 2012) in order not to mistake such responses for shallow conductive clay lenses. In practice, 100–200 m segments of data near power lines and roads are cut. The result of this processing is illustrated in Figure 3b where black lines show the remaining AEM soundings used for the inversion. For densely populated areas such as the NiCA survey area, up to 50% of the data has to be removed, but the remaining 50% of data still provides a large amount of useful information.

Once processed, the data are inverted with the quasi-3D method, spatially constrained inversion (SCI) (Viezzoli et al., 2008). Auken et al. (2008) show that as long as lateral slopes of the geologic layers are below 30%, i.e., well within slopes typically found in sedimentary areas, the quasi-3D model's description is sufficient to recover the true interface and layer resistivities. For the present data set, the spatial constraints were set to a factor of 1.35, meaning that resistivities of immediately adjacent soundings were allowed to change within roughly 35% from sounding to sounding. This constraint is considered loose; i.e., models can change very rapidly with very little adverse trade-off in the objective function of the inversion problem. Moreover, the spatial constraints were set to decrease rapidly outside a radius of 25 m from a sounding.

a) b)

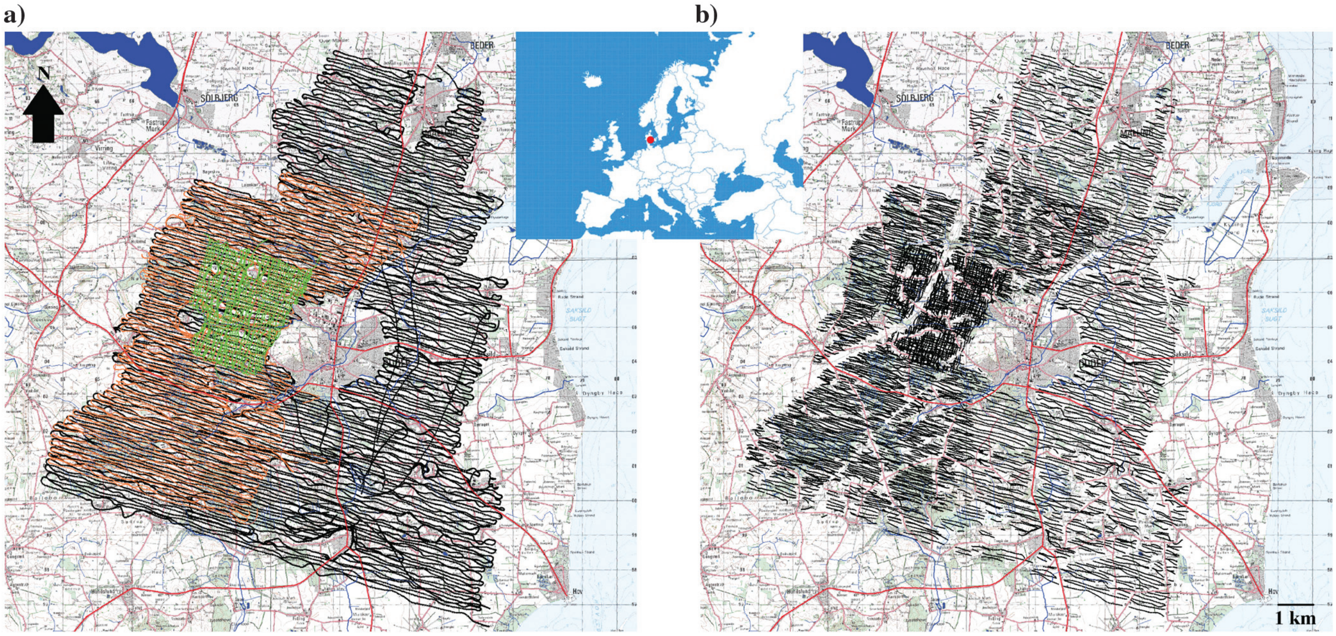

Figure 3. NiCA SkyTEM101 survey (20 km south from Aarhus, Denmark): (a) all lines showing three stages of data collection: Phase 1 (black) with 100-m spacing, phase 2 (orange) infill lines with 100-m spacing, and phase 3 (green), crosslines with 50-m line spacing and (b) soundings remaining after culling of the coupled data.

The total data set has more than 100,000 models, each one composed of 29 layers with fixed thicknesses increasing logarithmically within a depth range of 1.5–150 m (the first layers are 1.5-, 1.6-, 1.8-, 1.9-, 2.1-, and 2.2-m thick, and the last layer above the infinite half-space is 12.9-m thick). The resistivity is initially the same for all layers. A regularization constraint is applied to stabilize the inversion algorithm and to avoid under and overshoots in the resistivity model. We chose the multilayer modeling approach over few layer models with sharp boundaries because smooth modeling resolves small resistivity variations better, and a fixed number of layers does not have to be chosen beforehand (Auken and Christiansen, 2004).

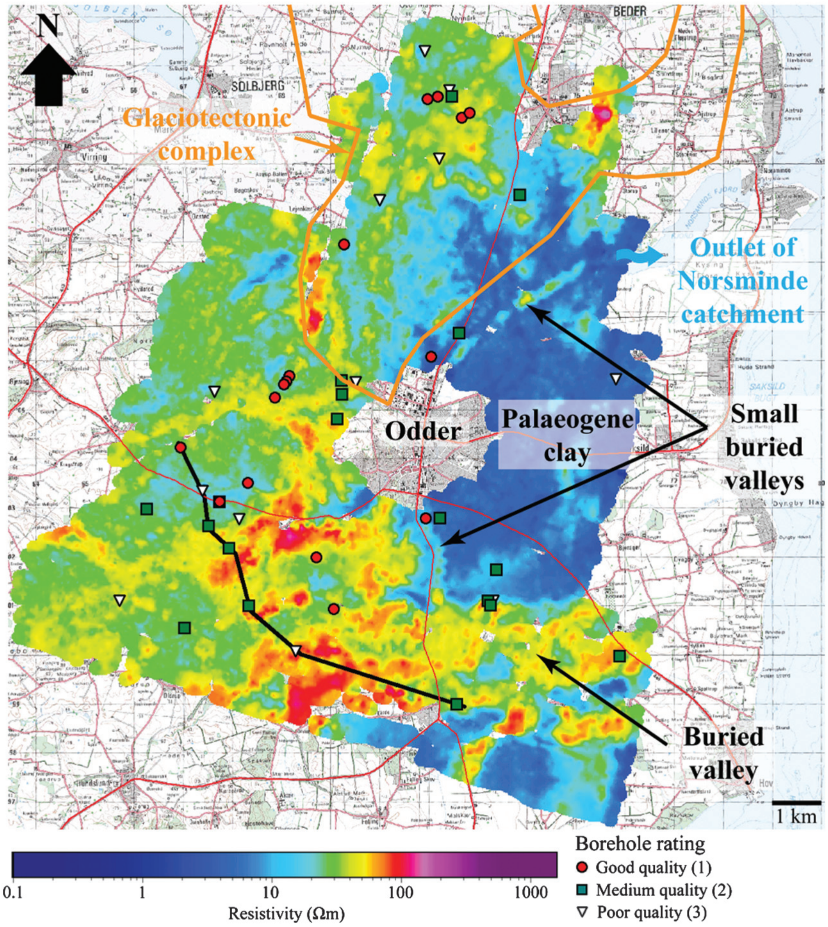

Figure 4. AEM results from the Norsminde catchment: mean resistivity map of the depth interval 15–20 m. Results are obtained after a spatially constrained inversion with 29 layers from 1.5 to 150-m depth. The map is obtained after kriging with a search radius of 150 m. The thick black line in the south corresponds to the profile whose section is displayed in Figure 6.

Results of the SCI are illustrated in Figure 4 with a mean resistivity map covering the 15–20-m depth interval. The resistivity grid is obtained using kriging with a search radius of 150 m and a grid spacing of 20 m. As well known from the physics of EM methods, conductive geologic units such as clay are better delineated than more resistive ones such as sand lenses. Blue to green colors correspond to low-to-intermediate resistivity values, typically fine-grained sediments with some clay content, and yellow to red colors correspond to high-resistivity values, typically coarse-grained sediments like sands. A clear difference is seen between the eastern and western parts of the survey area, with very low and uniform resistivity values on the eastern part, whereas the western part shows more complicated structures with alternating units. The eastern part has Palaeogene clay almost at the surface. These clays are conductive with a resistivity around 2 Ωm. Its top boundary is generally horizontal. The northwestern area delimited by the orange line in Figure 4 is a highly glaciotectonically deformed area where sand and clay layers have been thrust and folded. Many of the clay units comprise clay till whose resistivity levels are above those of the Palaeogene clay. Resistivities of this clay till are not far from sandy sediments like glaciofluvial sand and sand till, but different enough to separate clay units from sandy ones. Expected resistivity values for the different sediments in the region (Jørgensen et al., 2005) are displayed in Table 1. An extensive review can be found in Jørgensen et al. (2003). The determination of the resistivity values in Table 1 is based on direct comparison of borehole data with measured resistivities from TEM surveys, but also with resistivity log data. Measurements of resistivity values for different sediment types have also been conducted directly on borehole samples as detailed in Lykke-Andersen (1974) and Johnsen and Jørgensen (2006). The resistivity values of Table 1 have been confirmed by numerous studies, e.g., Høyer et al. (2011) and Jørgensen et al. (2012). Other geologic units such as buried subglacially meltwater-eroded tunnel valleys (Jørgensen and Sandersen, 2006), at different scales and filled with younger sediments, are also present in the area. One such very deep and wide buried valley extends from east to west through the southern part of the survey area (Figure 4).

Table 1. Resistivity ranges expected for the different geologic units (modified from Jørgensen et al., 2005).

Geologic unit	Symbol in Jupiter database	Resistivity range (Ωm)
Palaeogene clay	sl, ll, ol, etc.	1–10
Clay till	ml	25–60
Sand till	ms	>50
Meltwater sand and gravel	ds and dg	>60
Glaciolacustrine clay	dl	10–40
Miocene silt and sand	gi, gs, ki, ks,	>40
Miocene clay	gl	10–40
Sand	s	>40
Clay	l	1–60

RESULTS

Borehole data

Data from boreholes used in this study are stored in the Jupiter database maintained by the Geological Survey of Denmark and Greenland. A total of 551 boreholes (February 2011) are registered in the Jupiter database inside the survey area, yielding a density of 4.6 boreholes per km^2. The mean depth of the boreholes is 27 m.

These data comprise borehole construction logs (driller's logs), borehole sample descriptions, layer boundaries, depth, geographical coordinates, information about drilling method, purpose, groundwater head, etc. If the boreholes were logged by wireline tools, such results are also stored in the format of scanned documents and reports. Most boreholes were drilled for groundwater extraction, but many were drilled for geotechnical, raw material, and waste-site examination purposes. Only a very small number were drilled for scientific purposes.

Most boreholes are made by auger drilling, cable tool drilling, and mud-circulation drilling (ADITCL, 1997). The auger drillholes are typically shallow holes used for geotechnical, raw material, and waste-site examination. Normally, they have geologic log information of high quality. Cable tool drillholes are generally deeper and mainly used for water extraction wells. They, too, can offer high-quality geologic information. The mud-circulation drillholes can be split into two groups: direct circulation drillholes (rotary drillholes) and reverse mud-circulation drillholes (airlift drillholes). The direct circulation drillholes cannot provide quality data, whereas the reverse circulation drillholes typically provide reliable data, although not in the category of auger and cable tool drillholes. The quality of borehole samples achieved from the mud drillholes is strongly influenced by the bit used. Relatively big clay cuttings (up to about 15 cm) can be recovered from wing or blade bits, whereas only poor and disintegrated samples are derived when roller bits are used. In some cases, Ellog drillholes (Sørensen and Larsen, 1999) have been uploaded to the Jupiter database. The Ellog auger drilling method uses an integrated approach to obtain hydrological data where high-resolution gamma and resistivity logs are collected during drilling. At the same time, undisturbed depth-specific water samples can be taken through the cutting head.

The driller's log provides indispensable information such as the borehole method, the drill-bit type used, the sampling method, geographical coordinates, type of drilling mud used, weather, etc. In some cases, samples are collected for further description in laboratory. Because of the high complexity of the geology of the studied area, the accuracy of the coordinates is critical for the present comparison study. A substantial number of borehole coordinates were registered only after reading from a map. Only recent boreholes have their coordinates systematically determined by a global positioning system (GPS) and differential GPS.

Crosscheck method

Crosschecking of AEM results with borehole data is a two-step process involving (a) evaluation of borehole quality and (b) assessment of the match between boreholes and AEM models.

Borehole quality

To crosscheck the AEM results against the borehole data, only boreholes located close to the flight lines are used to minimize the effect of lateral geologic variations between the locations of the borehole and the AEM soundings. All boreholes located within ± 15 m from any sounding/flight line (30 m zone) were considered, which resulted in 54 boreholes. This is about 10% of the total number, despite the fact that the 30 m zone along the flight lines covers more than 40% of the area. The reason for this discrepancy in the number of boreholes finally selected is that many boreholes are situated close to buildings or roads, where the TEM data have either been culled due to couplings or not measured because the helicopter was not allowed to pass over buildings.

The selected 54 boreholes comprise a mixture of shallow auger drillings, deeper rotary and airlift drillings, and three Ellog drillings. The deeper mud-circulation drillings are made for water extraction, and the quality of their geologic descriptions varies significantly because some are made by air lift and some as direct rotary drillings. Many of the deeper boreholes do not have information on the drilling method, but it is likely that most of these are rotary drillings. For six of the boreholes, only borehole coordinates exist. At the end, we had 46 boreholes for the crosscheck (Figure 4). The mean depth of boreholes was 29 m.

When comparing AEM data to the borehole data, the quality of the latter is of utmost importance. If compared with poor borehole data, the results are useless in the best case, and in the worst case, they are misleading. We therefore performed a quality rating of the 46 boreholes, including handwritten driller's logs and potential inaccuracy in borehole coordinates. Some degree of subjectivity is involved in the rating, but we found no other way to evaluate the quality. Every effort was made to reduce subjectivity to keep the results transparent and documented.

To rate the borehole data, we considered the following parameters:

1) accuracy of geographic coordinates
2) degree of detail in geologic/lithological information derived, i.e., few described samples by driller and the number of selected samples for geologic description
3) accuracy of driller's sample descriptions, based on the level of detail, effort spent on descriptions, evaluation of the specific driller's skills, and general reputation
4) accuracy of the geologist's descriptions (if existing), based on the level of detail, quality of interpretation, effort spent on descriptions, evaluation of personal skills of the geologist in charge
5) objective information about drilling method, drilling purpose, age, etc.

These categories have each been assigned a rating falling in three levels: good (1), medium (2), and poor (3). At the end, the ratings are combined into an overall credibility rating in the same three levels. Figure 4 summarizes the ratings of boreholes by showing the location of good quality boreholes as red circles, medium quality boreholes as green squares, and poor quality boreholes as white inverted triangles.

Match between boreholes and AEM models

The actual matching was done by drawing a short (approximately 300 m) profile section along the flight line at each borehole and adding the geologic log and the AEM soundings to the profile. Then by using the expected resistivity values for sediments occurring in the area (Table 1), a visual comparison between the two data sets was performed. Finally, the comparison between the data sets was evaluated into four categories (Figure 5): a very good match (1), a good match (2), a poor match (3), and no match (4). These levels are evaluated in the following way:

1) A very good match can be assessed if the AEM models reproduce clay layers and sand layers at correct positions and with matching boundaries within a few meters.
2) A good match is given if the position of a clay/sand boundary is only somewhat imprecisely reproduced, e.g., 3–4 m at a depth of 15 m, or if thin layers are not resolved.
3) A poor match is given if there is still an overall resemblance between the distribution of sediments in the borehole and the resistivity values expected for these sediments, but if some discrepancy occurs in minor depth intervals.
4) If no match is given, no resemblance is observed.

Results of crosscheck

The results of the borehole rating showed that 34.8% of the boreholes were classified as good, 39.1% as medium, and 26.1% as poor (Figure 4). The mean rating of all 46 boreholes gave a value of 1.9, placing it just below medium.

The results of the crosscheck indicate a very good match for 43.5%, a good match for 32.6%, a poor match for 17.4%, and no match for 6.5% of the boreholes (Figure 5). Figure 6 shows an 8.5-km-long vertical profile section crossing the southern part of the area from west to east (segmented black line in Figures 4 and 5) with interpolated resistivities from the AEM soundings and seven of the boreholes used for the crosscheck. This profile was chosen so that it goes through a maximum number of boreholes with different qualities and through areas with different geologic configurations. Note that Palaeogene clay (dark blue color in the eastern part of the area in Figure 4) is difficult to penetrate by drilling, which limits the number of boreholes and makes the depth of the boreholes, if existing, very shallow where the clay reaches the surface. The corresponding borehole rating and the given match at each location is indicated above each borehole in Figure 6. On the profile, all levels of matches and borehole ratings are shown. In general, a close match between the borehole data and the AEM data is evident. Details of four of the boreholes (nos. 1, 2, 3, and 6) are shown in Figures 7 and 8 to exemplify the comparison analysis with short profiles of 300 m.

Borehole no. 1 (Jupiter archive no. 98.1319) shown in Figure 7 is a relatively new borehole constructed for a groundwater resource mapping and protection program. Despite using mud-circulation drilling, the quality of this borehole is rated good because of other

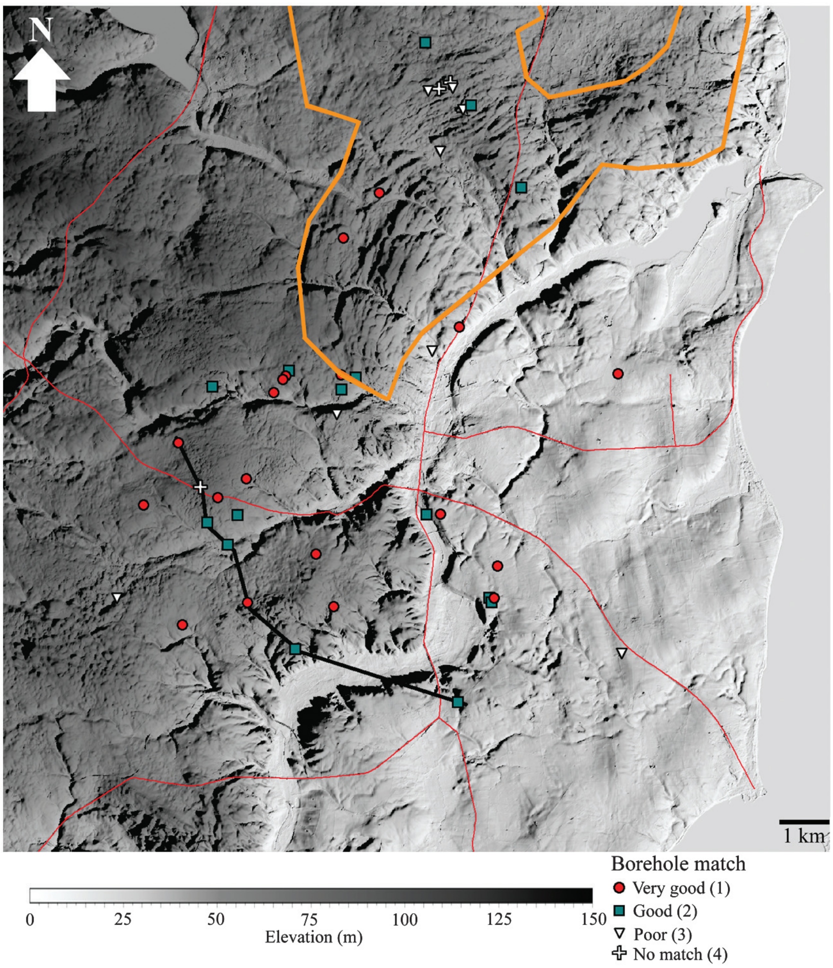

Figure 5. Borehole match with AEM results superimposed on shaded-relief topography. The thick black line in south corresponds to the profile displayed in Figure 6. The orange polygon delimits the glaciotectonic complex where arc-shaped deformations in the surface are clearly visible. Red lines show main roads.

criteria: sampling, descriptions, interpretation, location etc. The open borehole was logged (prior to casing and sealing) with induction, resistivity, and gamma tools (Orbicon A/S, 2012). The match is found to be very good because the clay till layer (ml) in the top 37 m in the AEM soundings is found to have a resistivity of 25–50 Ωm, which is consistent with the values in Table 1. Also the two resistivity transitions toward higher values at elevations of about 60 and 47 m in the induction log match the resistivity transitions visible in AEM results quite well, despite the smoothness of the inverted models (Figure 7). A 5-m-thick sand till layer (ms) is, however, not reproduced in the AEM resistivity models. This layer is relatively thin compared to its overburden (20 m). The occurrence of the sand till layer is based on laboratory examination of a small part of the entire collected borehole samples, but according to on-site geologic descriptions of the full samples made by the borehole logging company (Orbicon A/S, 2012), the sand till does not exist; instead, it is described to be also clay till (however, a bit more sandy). The lower boundary of the clay till (ml) fits exactly with the top of the 50-Ωm layer in the AEM soundings located around 45-m elevation. The induction and Ellogs also show close agreement with resistivities between 15 and 40 Ωm in the clay till package. Miocene sand below is medium grained and well sorted. AEM models show higher resistivities of about 50–70 Ωm, a value also measured by induction logs. At an elevation of 5 m, the borehole encounters Miocene silty clay (gl), which, according to the induction log, has a resistivity of about 20 Ωm. This layer corresponds to a decrease in resistivity in the AEM data. At this depth, there is not much signal left because the estimated DOI (Christiansen and Auken, 2012) is situated above this level.

Another example is borehole no. 2 (JA# 98.448) shown in Figure 8a. This borehole is relatively old (1980). There is not much information about the drilling method, and the correct location of the borehole cannot be verified. There is no geologic sample description or interpretation, only the driller's own description, which is not thorough. The overall validity of the borehole data is therefore rated as poor. As seen in Figure 8a, there is not a good match in the top 20 m to the AEM model. The clay layer in the top 10 m falls within high AEM resistivities, whereas the sandier interval below occurs in the transition zone to more conductive layers suggested in AEM soundings. The high resistivities emerging at depths of about 40 m are not confirmed by the borehole. The resulting evaluation is that there is no match.

Borehole no. 3 (JA# 99.803) is a newly airlift-drilled water well (Figure 8b). We noted the quality of this borehole as medium because there is some uncertainty related to its geographic coordinates, and the geologic descriptions and interpretation are not of top quality. The match between the borehole and AEM models is evaluated as good. The reason why it is not evaluated very good is that AEM soundings show a 25-m thickness of the clay till layer compared to the 33 m shown by the borehole. Otherwise, the clay till (ml) is nicely mapped in AEM soundings by a 25–50-Ωm layer, followed by a deeper layer with resistivities of 50–100 Ωm reflecting a layer of medium to coarse-grained meltwater sand (ds) in the borehole. In the lower part, silty Miocene sediments (gi) are followed by slightly decreasing resistivities in AEM soundings. The slight misfit of the boundary between the clay till and the sand is due to difficulties in precisely resolving the boundary between the clay till (ml) and meltwater sand (ds) in the AEM data.

The last borehole no. 6 (JA# 108.189), shown in Figure 8c, is of very low quality. A rotary drill was used, with an insufficient driller's description and report. Geologic descriptions are performed well, but are useless because the descriptions are done on samples achieved from unreliable drilling and sampling methods. As seen in Figure 8c, the elevation of the borehole is wrong (4 m above ground

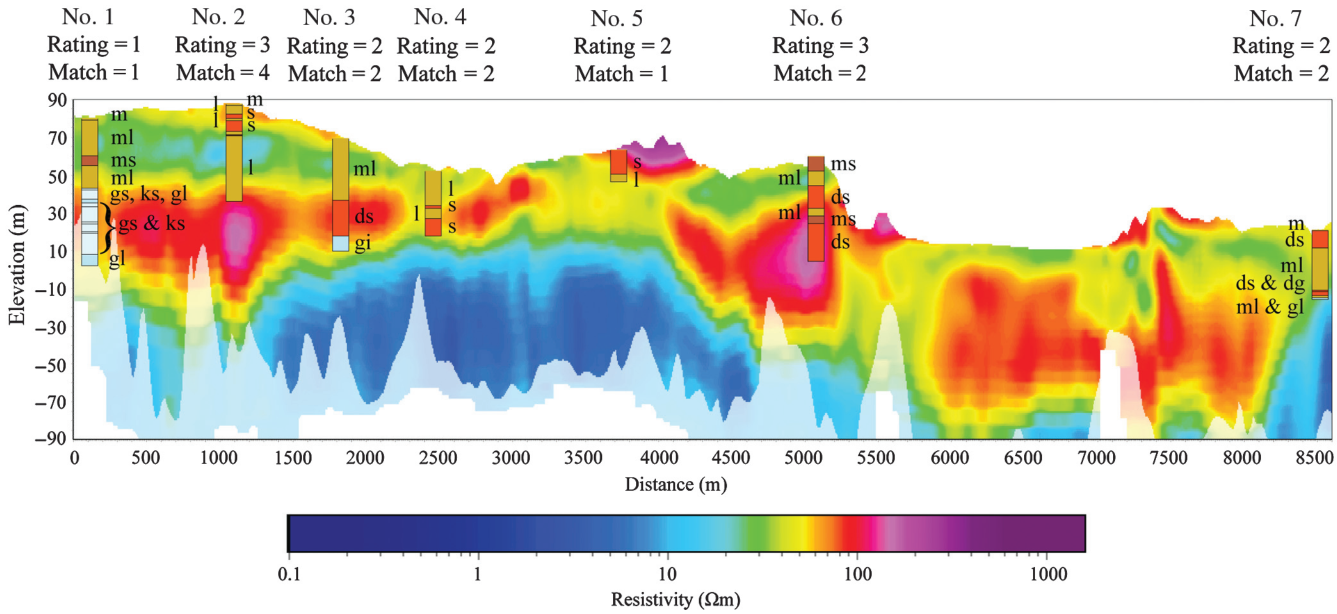

Figure 6. Resistivity section along the nonstraight profile shown in Figure 4. The AEM resistivities are obtained from a smooth SCI with 29 layers (first layer is 1.5-m thick and the deepest interface is at 150-m), and after kriging with a 150 m search radius and a grid spacing of 20 m. Borehole data are superimposed with lithology description (summarized in Table 1 with estimated resistivities, the m symbol corresponds to top soil). The faded colors correspond to parts of the section that are below the estimated DOI (i.e., below black lines in Figures 7 and 8). Note that the color scale in borehole logs is indicative and not the same as the resistivity color scale.

level). The upper 8 m is described as sand till (ms), followed by 10 m of clay till (ml). The corresponding resistivity values are between 23 and 37 Ωm, highest at the surface, at the sand till. This relatively low resistivity in the first layer of the TEM resistivity model compared to the borehole data is likely due to the regularization scheme of the inversion process, i.e., the vertical constraints of the multilayer inversion, which smoothen sharp transitions from thin resistors to conductive layers. However, an elevated resistivity is still detected in the near surface. Except for 4 m of clay till (ml) in the middle part of the borehole, the high-resistivity levels here (60–160 Ωm) correspond to meltwater sand (ds). The match is evaluated as good. The reason for the slight discrepancy in the upper 8 m may be caused by poor borehole data.

Discussion of crosscheck results

The overall results showed a very good or good match in 76.1% of the crosschecks, leaving 23.9% having a poor or no match. For the category of poor match, however, there were still some resemblances with the main geologic units. Cases with no match amount to 6.5%. The match at each borehole was evaluated without taking the borehole data quality into account. To achieve a correct picture of the system's capability to map the near-surface geology, the crosscheck should principally be made against high-quality boreholes without errors and misleading information. To get closer to the real picture, we have therefore examined the reasons behind each mismatch by taking the borehole quality rating into account. If the mismatch is caused by wrong or poor borehole data, the matching results should be adjusted accordingly.

Evaluated causes for mismatch between AEM and borehole data have been sorted into the following five groups (results summarized in Table 2):

1) poor borehole data quality due to poor samples, descriptions, borehole method, driller's log, etc.
2) occurrence of vertical geologic variations
3) occurrence of lateral geologic variations
4) imprecision in borehole coordinates
5) unknown or other causes.

Probable explanations were found for the mismatches at 30 locations (major and minor mismatches). At five of these locations, we estimate the cause to be lateral variations (group 3) mainly occurring from glaciotectonic deformation. Because the glaciotectonic complex consists of stacked, thrust, and folded layers in a strong heterogenic mixture, the AEM data and the applied SCI inversion method will experience problems resolving the geology in detail within this highly complicated area. The distribution of boreholes with match values is shown in Figure 5, where the orange line shows the extension of the glaciotectonic complex. Six of 11 boreholes with poor or no match are found in this area and two others are very close to it. Also, four out the five boreholes at which lateral variations were believed to be the cause of mismatches are situated within this area. Outside, the geology is consistent between AEM and borehole data, although the geologic complexity is relatively high there as well.

Limited vertical resolution (group 2) is believed to be the reason for mismatch at seven locations and is caused by the presence of layers, which are too thin to be resolved by the system, due to inherent limitations of resolving capabilities of the EM method (see details in the section "Sensitivity and performance analysis based on synthetic cases").

Poor borehole data quality (group 1) is expected to be the cause of mismatch at 11 locations, and imprecise borehole coordinates (group 4) are likely the cause at four locations.

In summary, 50% of the mismatches are related to the boreholes (groups 1 + 4) and not to the limitations of the AEM system (groups 2 + 3). The proportion of poor match and no match together should therefore be reduced from 23.9% to about 12%. If we exclude the glaciotectonic complex in the comparison analysis because of its highly complicated geology, this number is further reduced.

Regarding the very first few meters of the ground, the comparison with boreholes is challenging due to the high spatial variability of this uppermost part, which is often rearranged and tilled by human activities. Only comparison with ground-based measurements exactly along the flight lines would allow such a crosscheck. However, it is certain that any AEM system, in frequency and time domains, has limitations in the resolution of the first 2–3 m (as shown in the section "Sensitivity and performance analysis based on synthetic cases") because of the flight altitude itself, which is almost never below 30 m, except in very open and unpopulated areas where it may go down to 20 m. Only ground-based (or towed)

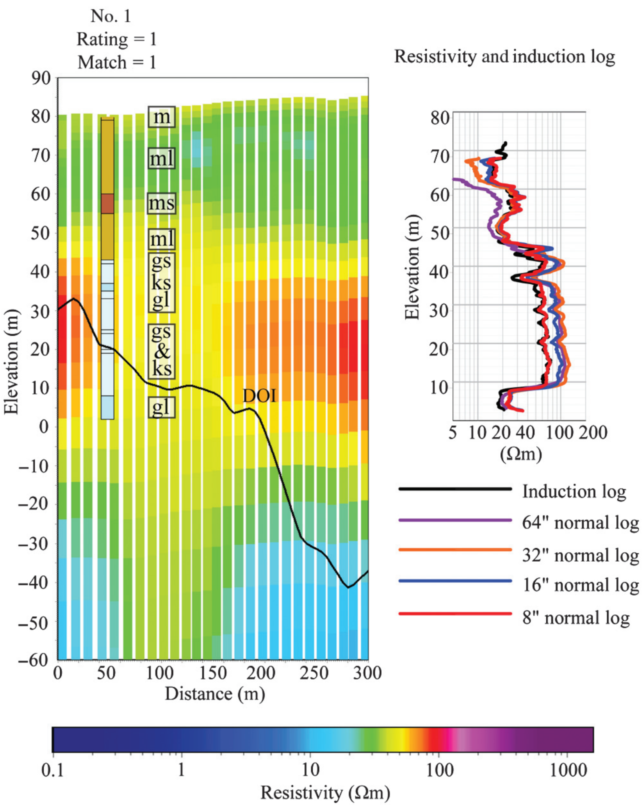

Figure 7. Comparison with resistivity and induction logs at borehole no. 1 (cf. Figure 6): on the left the borehole lithology with the nearest AEM soundings (the discretization corresponds to the one used during the SCI), the dark line indicates the estimated DOI and on the right the resistivity and induction logs. Lithology description in the geologic log is summarized in Table 1 with estimated resistivities (*m* symbol corresponds to top soil). Note that the color scale in the borehole log is indicative and not the same as the resistivity color scale.

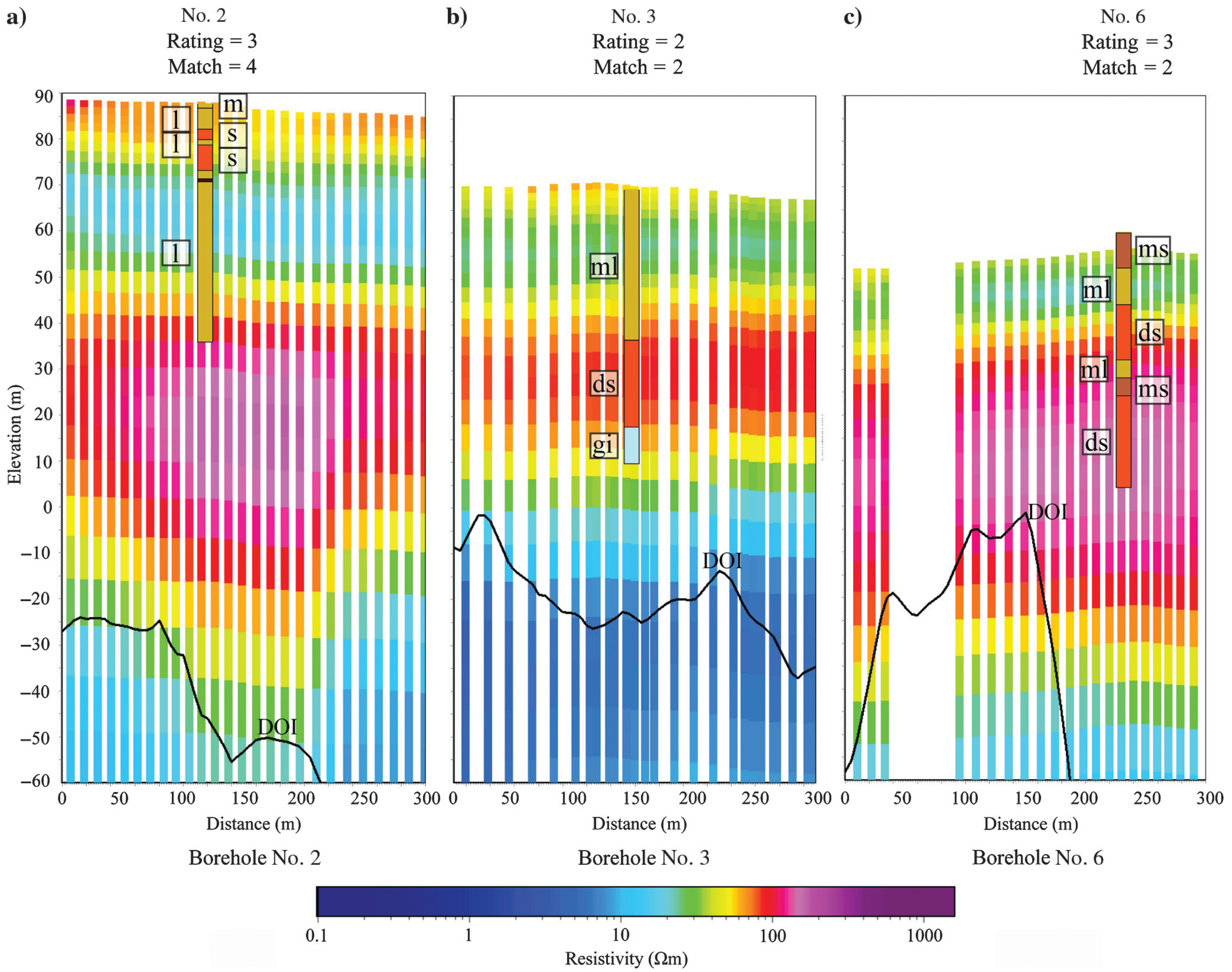

Figure 8. Three selected crosscheck panels with boreholes also displayed in Figure 6. The difference with Figure 6 is that AEM resistivities are not coming from gridded resistivity maps, but are direct projections of the resistivity models from the AEM soundings, which are closer than 15 m from the profile. See Figure 7 for additional explanations.

Table 2. Statistics on the reason for mismatch with the borehole database, for 30 observations within the boreholes having overall matching levels of good, poor, and no when compared to AEM results.

Reason of mismatch	Occurrence (observations/%)
Borehole data (quality of samples and descriptions/geologic interpretations)	11/36.7
Vertical geologic variations (vertical resolution)	7/23.3
Lateral geologic variations (horizontal resolution)	5/16.7
Inaccuracy in borehole coordinates	4/13.3
Other/unknown	3/10.0

systems would allow a better near-surface resolution, but they do not allow easy accessibility and fast coverage such as AEM methods do.

CONCLUSION

The new HTEM system presented in this paper brings airborne transient EM methods to the level of near-surface resolution so far reachable only with HFEM systems. The presented borehole rating technique allowed us to evaluate the match with the AEM data set pertinently, by considering the quality of the boreholes and by pinpointing the cases where a mismatch is likely due to poor borehole quality. The methodology also allows the use of conventional borehole data such as geologic logs for the assessment of AEM data, without being limited to conductivity logs.

Despite the high complexity of parts of the survey area where geologic layers have been glaciotectonically thrust and folded, an overall good fit with at least three-quarters of the boreholes has been found. The remaining quarter of the borehole-AEM mismatches falls into two groups: Half of them are due to inaccurate borehole coordinates (in comparison with the local spatial variability of the geology) or a bad borehole quality (i.e., borehole rating of 3); the remaining mismatches, one-eighth of all boreholes, are due to strong lateral or vertical geologic variations (within a few meters) in the very center of the glaciotectonic complex, which cannot be resolved by the transient AEM system.

Our findings show that HTEM systems such as SkyTEM101 provide a reliable and high resolution of even very shallow geologic layers. Combined with their fast and dense coverage, these systems are cost-effective alternatives to ground-based geophysical systems or boreholes for a wide range of applications such as mapping of raw materials for the construction industry, geotechnical applications such as road constructions, and vulnerability estimations in groundwater resource mapping.

ACKNOWLEDGMENTS

We are grateful to the Danish Council for Strategic Research who supported the development of the time-domain system and the algorithm developments and who made it possible to carry out the large field test. The support was given to the Nitrate Reduction in a Geologically Heterogeneous Catchment (NiCA) project (www.nitrat.dk), funded under contract no. DSF 09-067260.

REFERENCES

ADITCL, 1997, Drilling: The manual of methods, applications, and management: By the Australian Drilling Industry Training Committee Ltd.: Lewis Publishers.

Auken, E., and A. V. Christiansen, 2004, Layered and laterally constrained 2D inversion of resistivity data: Geophysics, **69**, 752–761, doi: 10.1190/1.1759461.

Auken, E., A. V. Christiansen, L. Jacobsen, and K. I. Sørensen, 2008, A resolution study of buried valleys using laterally constrained inversion of TEM data: Journal of Applied Geophysics, **65**, 10–20, doi: 10.1016/j.jappgeo.2008.03.003.

Auken, E., N. Foged, and K. I. Sørensen, 2010, Approaching 10 microsec (and earlier) with the SkyTEM system: ASEG Extended Abstracts, **1**, 1, doi: 10.1071/ASEG2010ab280.

Baldridge, W. S., G. L. Cole, B. A. Robinson, and G. R. Jiracek, 2007, Application of time-domain airborne electromagnetic induction to hydrogeologic investigations on the Pajarito Plateau, New Mexico, USA: Geophysics, **72**, no. 2, B31–B45, doi: 10.1190/1.2437701.

Christiansen, A. V., and E. Auken, 2012, A global measure for depth of investigation: Geophysics, **77**, no. 4, WB171–WB177, doi: 10.1190/geo2011-0393.

Christiansen, A. V., E. Auken, and A. Viezzoli, 2011, Quantification of modeling errors in airborne TEM caused by inaccurate system description: Geophysics, **76**, no. 1, F43–F52, doi: 10.1190/1.3511354.

Dahlin, T., 2001, The development of DC resistivity imaging techniques: Computers & Geosciences, **27**, 1019–1029, doi: 10.1016/S0098-3004(00)00160-6.

Dickinson, J. D., D. R. Pool, R. W. Groom, and L. J. Davis, 2010, Inference of lithologic distributions in an alluvial aquifer using airborne transient electromagnetic surveys: Geophysics, **75**, no. 4, WA149–WA161, doi: 10.1190/1.3464325.

Donohue, S., M. Long, P. O'Connor, T. E. Helle, A. A. Pfaffhuber, and M. Rømoen, 2012, Multi-method geophysical mapping of quick clay: Near Surface Geophysics, **10**, 207–219, doi: 10.3997/1873-0604.2012003.

Everett, M. E., 2012, Theoretical developments in electromagnetic induction geophysics with selected applications in the near surface: Surveys in Geophysics, **33**, 29–63, doi: 10.1007/s10712-011-9138-y.

Foged, N., E. Auken, A. V. Christiansen, and K. I. Sørensen, 2013, Test site calibration and validation of airborne and ground based TEM systems: Geophysics, **78**, no. 2, E95–E106, doi: 10.1190/geo2012-0244.1.

Høyer, A.-S., H. Lykke-Andersen, F. Jørgensen, and E. Auken, 2011, Combined interpretation of SkyTEM and high-resolution seismic data: Physics and Chemistry of the Earth, **36**, 1386–1397, doi: 10.1016/j.pce.2011.01.001.

Johnsen, R., and F. Jørgensen, 2006, Undersøgelser af sammenhængen mellem moræners sedimentologiske og elektrisk ledende egenskaber — herunder estimering af grænsen mellem ler og "ikke-ler" ATV — Jord og grundvand, Vintermøde, 7. — 8. martys 2006.

Jørgensen, F., E. Auken, and K. I. Sørensen, 2003, Anvendelse af TEM-metoden ved geologisk kortlægning. GeoFysikSamarbejdet: Aarhus Universitet.

Jørgensen, F., P. Sandersen, E. Auken, H. Lykke-Andersen, and K. I. Sørensen, 2005, Contributions to the geological mapping of Mors, Denmark — A study based on a large-scale TEM survey: Bulletin of the Geological Society of Denmark, DGF, **52**, 53–75.

Jørgensen, F., and P. B. E. Sandersen, 2006, Buried and open tunnel valleys in Denmark-erosion beneath multiple ice sheets: Quaternary Science Reviews, **25**, 1339–1363, doi: 10.1016/j.quascirev.2005.11.006.

Jørgensen, F., W. Scheer, S. Thomsen, T. O. Sonnenborg, K. Hinsby, H. Wiederhold, C. Schamper, B. Roth, R. Kirsch, and E. Auken, 2012, Transboundary geophysical mapping of geological elements and salinity distribution critical for the assessment of future sea water intrusion in response to sea level rise: Hydrology and Earth System Sciences, **16**, 1845–1862, doi: 10.5194/hess-16-1845-2012.

Lane, R., D. Heislers, and P. McDonald, 2001, Filling in the gaps — Validation and integration of airborne EM data with surface and subsurface observations for catchment management — An example from Bendigo, Victoria, Australia: ASEG Extended Abstracts, 1–4, doi: 10.1071/ASEG2001ab067.

Lavoué, F., J. Van Der Kruk, J. Rings, F. Andre, D. Moghadas, J. A. Huisman, S. Lambot, L. Weihermüller, J. Vanderborght, and H. Vereecken, 2010, Electromagnetic induction calibration using apparent electrical conductivity modelling based on electrical resistivity tomography: Near Surface Geophysics, **8**, 553–561, doi: 10.3997/1873-0604.2010037.

Lykke-Andersen, H., 1974, Kortlægning af undergrunden i omegnen syd og vest for Århus Undersøgelser af Århusegnens undergrund: Undersøgelser af Århusegnens undergrund.

Mullen, I. C., K. E. Wilkinson, R. G. Cresswell, and J. Kellett, 2007, Three-dimensional mapping of salt stores in the Murray-Darling Basin, Australia: 2. Calculating landscape salt loads from airborne electromagnetic and laboratory data: International Journal of Applied Earth Observation and Geoinformation, **9**, 103–115, doi: 10.1016/j.jag.2006.08.005.

Oluwafemi, O., and M. A. Oladunjoye, 2013, Integration of surface electrical and electromagnetic prospecting methods for mapping overburden structures in Akungba-Akoko, Southwestern Nigeria: International Journal of Science and Technology, **2**, 122–147.

Orbicon A/S, 2012, NST Aarhus Undersøgelsesboringer, Solbjerg Fillerup (unpublished report).

Pfaffhuber, A. A., E. Grimstad, U. Domaas, E. Auken, N. Foged, and M. Halkjaer, 2010, Airborne EM mapping of rockslides and tunneling hazards: The Leading Edge, **29**, 956–959, doi: 10.1190/1.3480009.

Podgorski, J. E., E. Auken, C. Schamper, A. V. Christiansen, T. Kalscheuer, and A. G. Green, 2013, Processing and inversion of commercial helicopter time-domain electromagnetic data for environmental assessments and geologic and hydrologic mapping: Geophysics, **78**, no. 4, E149–E159, doi: 10.1190/geo2012-0452.1.

Refsgaard, J. C., E. Auken, C. A. Bamberg, B. S. B. Christensen, T. Clausen, E. Dalgaard, F. Effersø, V. Ernstsen, F. Gertz, A. L. Hansen, X. He, B. H. Jacobsen, K. H. Jensen, F. Jørgensen, L. F. Jørgensen, J. Koch, B. Nilsson, C. Petersen, C. Petersen, G. De Schepper, C. Schamper, K. I. Sørensen, R. Therrien, C. Thirup, and A. Viezzoli, 2014, Nitrate reduction in geologically heterogeneous catchments — A framework for assessing the scale of predictive capability of hydrological models: Science of the Total Environment, **468–469**, 1278–1288, doi: 10.1016/j.scitotenv.2013.07.042.

Reid, J. E., and J. Vrbancich, 2004, A comparison of the inductive-limit footprints of airborne electromagnetic configurations: Geophysics, **69**, 1229–1239, doi: 10.1190/1.1801939.

Röttger, B., R. Kirsch, R. Friborg, W. Scheer, S. Thomsen, and W. Voss, 2005, Multifrequency airborne EM surveys — A tool for aquifer vulnerability mapping, *in* D. K. Butler, ed., Near-surface geophysics: SEG.

Schamper, C., and E. Auken, 2012, Mini-SkyTEM: A new airborne transient EM system for near-surface aquifer mapping: Presented at Near Surface Geoscience — Remote Sensing Workshop.

Schamper, C., E. Auken, and K. Sørensen, 2014, Coil response inversion for very early time modeling of helicopter-borne time-domain electromagnetic data and mapping of near-surface geological layers: Geophysical Prospecting, **62**, 658–674, doi: 10.1111/1365-2478.12104.

Schamper, C., J. B. Pedersen, N. Foged, A. V. Christiansen, K. I. Sørensen, and E. Auken, 2011, Refinement of the national TEM reference model at Lyngby Department of Geoscience: Aarhus University.

Schamper, C., F. Rejiba, and R. Guérin, 2012, 1D single-site and laterally constrained inversion of multifrequency and multicomponent ground-based electromagnetic induction data — Application to the investigation of a near-surface clayey overburden: Geophysics, **77**, no. 4, WB19–WB35, doi: 10.1190/geo2011-0480.1.

Sørensen, K. I., and E. Auken, 2004, SkyTEM — A new high-resolution helicopter transient electromagnetic system: Exploration Geophysics, **35**, 194–202, doi: 10.1071/EG04194.

Sørensen, K. I., and F. Larsen, 1999, Ellog Auger drilling: 3-in-one method for hydrogeological data collection: Ground Water Monitoring & Remediation, **19**, 97–101, doi: 10.1111/j.1745-6592.1999.tb00245.x.

Steuer, A., B. Siemon, and E. Auken, 2009, A comparison of helicopter-borne electromagnetics in frequency- and time-domain at the Cuxhaven valley in Northern Germany: Journal of Applied Geophysics, **67**, 194–205, doi: 10.1016/j.jappgeo.2007.07.001.

Supper, R., I. Baron, D. Ottowitz, K. Motschka, S. Gruber, E. Winkler, B. Jochum, and A. Römer, 2013, Airborne geophysical mapping as an innovative methodology for landslide investigation: Evaluation of results from the Gschliefgraben landslide, Austria: Natural Hazards and Earth System Sciences, **13**, 3313–3328, doi: 10.5194/nhess-13-3313-2013.

Tarantola, A., and B. Valette, 1982, Generalized nonlinear inverse problems solved using a least squares criterion: Reviews of Geophysics and Space Physics, **20**, 219–232, doi: 10.1029/RG020i002p00219.

Tekzan, B., 1999, A review of environmental applications of quasi-stationary electromagnetic techniques: Surveys in Geophysics, **20**, 279–308, doi: 10.1023/A:1006669218545.

Viezzoli, A., A. V. Christiansen, E. Auken, and K. I. Sørensen, 2008, Quasi-3D modeling of airborne TEM data by spatially constrained inversion: Geophysics, **73**, no. 3, F105–F113, doi: 10.1190/1.2895521.

Viezzoli, A., F. Jørgensen, and C. Sørensen, 2012, Flawed processing of airborne EM data affecting hydrogeological interpretation: Ground Water, **51**, 191–202, doi: 10.1111/j.1745-6584.2012.00958.x.

Vrbancich, J., and P. K. Fullagar, 2004, Towards seawater depth determination using the helicopter HoistEM system: Exploration Geophysics, **35**, 292–296, doi: 10.1071/EG04292.

Vrbancich, J., and P. K. Fullagar, 2007, Improved seawater depth determination using corrected helicopter time-domain electromagnetic data: Geophysical Prospecting, **55**, 407–420, doi: 10.1111/j.1365-2478.2007.00602.x.